# Electron-enhanced high power impulse magnetron sputtering with a multilevel high power supply: Application to Ar/Cr plasma discharge

J. Zgheib, L. Berthelot, J. Tranchant, N. Ginot, M.-P. Besland, A. Caillard, T. Minea, A. Rhallabi, P.-Y. Jouan

# Electron-enhanced High Power Impulse Magnetron Sputtering with a multi-level high power supply. Application to Ar/Cr plasma discharge.

J. Zgheib[1*], L. Berthelot[1], J. Tranchant[1], N. Ginot[2], M-P. Besland[1], A. Caillard[4], T. Minea[3], A. Rhallabi[1] and P-Y. Jouan[1*]

[1] CNRS- IMN Institut des Matériaux de Nantes Jean Rouxel, Nantes University

[2] IETR - Institut d'Électronique et des Technologies du numéRique, Nantes University

[3] LPGP- Laboratoire de Physique des Gaz et des Plasmas, Université Paris-Saclay, CNRS, Orsay, France

[4] GREMI- Groupe de Recherche sur les Milieux Ionisés, Orléans

[*]joelle.zgheib@cnrs-imn.fr

[*]pierre-yves.jouan@cnrs-imn.fr

## Abstract

A High Power Impulse Magnetron Sputtering (HiPIMS) power supply, called e-HiPIMS, has been developed and used to deposit chromium thin films within an argon discharge. This power supply comprises three stages; each can deliver a voltage pulse up to 300 V. The advantage of this power supply is the possibility of tailoring a pulse waveform on the cathode with several voltage levels. This e-HiPIMS can operate in the standard HiPIMS mode (s-HiPIMS) and multi-pulse HiPIMS mode (m-HiPIMS). Each voltage sequence is independently managed regarding width, delay, and voltage level. They can all be synchronized, giving the standard HiPIMS, or shifted in time and added to each other. Hence, the idea is to favor a specific ion population compared to others, according to the process needs and the targeted application. A beneficial example used a three-pulse sequence with different voltage levels. The influence on the temporal behavior of the plasma parameters, namely currents and electron energy, has been studied for each pulse sequence. The results show that the discharge current stays within the same order of magnitude as in the standard HiPIMS. The reference current level can be obtained quickly, adding a short over-pulse, even if its voltage level is relatively low. Furthermore, measurements by the Langmuir probe reveal that a maximum electron density is obtained at 0.2 Pa and 0.6 Pa of argon for a configuration

that adds two distinguished voltage-pulse sequences, one between 5-15 µs and the last between 20-40 µs. It comes out that this e-HiPIMS sequence significantly increases the electron density.

## I. Introduction

Magnetron sputtering is a widespread process for thin film deposition, allowing to tune in a wide range structural, electrical and mechanical properties of deposited films. Commonly known as Physical Vapor Deposition (PVD), the physical sputtering of a target under energetic ion bombardment generated by a plasma discharge is a process widely used in many technological domains such as microelectronics[1], photovoltaics[2,3], biology,[4,5] or mechanics,[6] among other fields. Moreover, adding a reactive gas such as oxygen or nitrogen[7–11,] allows to enlarge the panel of deposited material and open the way to a wider range of materials and applications.

Conventional direct current (DC) or radio frequency (RF) plasma-based magnetron sputtering have shown some limitations. Hence, nowadays, the request for thin film properties has increased in a wide extend of targeted electrical and structural properties. To obtain denser layers with enhanced properties associated with a good surface conformity, the generation of a discharge with a high ionization degree and very energetic ions is needed. Moreover, a high density of ionized species extracted from the target are highly needed to reach dense coatings[12]. In the meantime, such energetic conditions can damage the substrate and promote an important increase of the substrate temperature, which might be unsuitable for sensitive substrates like polymers or specific materials and devices.

To circumvent such drawback, an alternative way emerged is the beginning of this 2000's [13–15] with high voltage and high-current magnetron discharge, so called High Power Impulse Magnetron Sputtering (HiPIMS) that has been classified in the ionized-PVD plasma processing technologies. Such power supply allows to generate a very dense plasma with a very high degree of ionization degree of sputtered atoms from the target thanks to a few tens microseconds pulse duration (typically in the 30 to 100 µs range) at a high frequency up to a few kHz. The generation of such a dense plasma in a very short period requires instantaneous powers of some tens of kW. The interest of HiPIMS discharges has been demonstrated in many studies[8,16,17] highlighting how the enhancement of the ionization degree of the sputtered

particles can promote a huge effect on the microstructure and functional properties of the deposited films.

To get more understanding on the electrical characteristics of the discharge and a higher control of the neutral and ion transport phenomena as well as their effects on the thin film growth mechanisms, a large panel of experimental investigations has been performed using Langmuir probes[9,18,19], Optical Emission Spectroscopy,[20] and Mass Spectroscopy[21], among many others[22]. These different studies demonstrated the high ionization degree of sputtered species about two orders of magnitude as compared to the typical values of conventional magnetron discharges. The first effect is thus the huge ionization fraction of the sputtered species that can, in particular experimental conditions, exceed 90% of the discharge.[21,23] Such high ionization degree of sputtered species leads to a very directional ionized discharge leading to a highly oriented film with a typical columnar structures perpendicular to the substrate. Such process allows to enhance the deposition conformity of the deposited film on 3D patterned surfaces such as trenches or via structures with a high aspect ratio.[24]

In most cases, publishes results revealed that the dominant population is the sputtered ionized metal species ($M^+$) as compared to the argon ion population ($Ar^+$). Indeed, the pulse shape applied to the target directly affects the electrical behavior of the HiPIMS discharge and the time evolution of ions and neutrals densities. Ina previous study, the effects of the duty cycle, i.e. time on ($t_{on}$) and time off ($t_{off}$), on the temporal evolution of the electron density and electron temperature, as well as the ion and neutral densities, have been analyzed.[21] Moreover, the authors demonstrated that the densities of double-charged ions ($Ar^{2+}$ and $M^{2+}$) could be more significant.[21]

In addition, in the previous decade, other configurations of the instantaneous voltage applied to the target have been investigated. The effect of HiPIMS multi-pulse (m-HiPIMS) was studied[25,26] and brought more information on the mechanisms involved in the deposition process. The first advantage of m-HiPIMS is to provide a better control of the discharge parameters than a standard HiPIMS (s-HiPIMS) process.[25,27] O. Antonin at al. [25] investigated the effect of five high voltage micro-pulses of 3µs separated by varying delays time ($t_{off}$) at different frequencies to guarantee the same average power. As a result, they observed an increase of the deposition rate by 50%, and an enhancement of the ionization rate within the discharge, leading to a higher content of sputtered metallic species. Moreover, in further work of M. Fekete et al.[26], it is demonstrated that the ion flux significantly increases compared to s-HiPIMS with tightly dependency on the delay between pulses ($t_{off}$). In addition, at high

pressure, remote probe measurements revealed a peak density after the power pulse, significant of a slow and diffusive ion transport.

Other HiPIMS configuration including the association of different pulses, so-called bipolar pulse, has been further investigated. [7,20,28,29]: a small positive pulse was added after the high-power initial negative pulse on the target. Such HiPIMS configuration allows the increase of the sputtered ions energy.

On the basis of these previous works, we developed a new HiPIMS power supply, so-called e-HiPIMS for electron enhanced HiPIMS that associate a standard HiPIMS (s-HiPIMS) and the multi-pulse HiPIMS (m-HiPIMS). Such power supply allows to deliver multi-voltage pulses separated by various and tuned $t_{0ff}$ values during the $t_{on}$ period. After a first stage of discharge studies, we investigated the effect of such supply on a pure Ar discharge with a chromium target. Our objective has been to tune the pulse shape in order to amplify only a specific ion population compared to the other plasma species. Indeed, previous studies[30] have shown that in HiPIMS discharges, the peak density associated to each ion population can be shifted at different time occurrence during the main voltage pulse. As shown in previous work[21], during the pulse time-on $t_{on}$ in a HiPIMS pure Ar discharge involved with a chromium (Cr) target, the $Ar^+$ peak density appears first followed by $Cr^+$ peak. Our hypothesis is thus to add a pulse at the moment of maximum density of an ion species assuming that this species density might be amplified. As an illustration, apply an over-pulse synchronized either with the maximum of $Ar^+$ density or with the $Cr^+$ maximum density, and then observe if any effects on the structural and chemical properties of the deposited films.

It is well known and established that an increase of $Ar^+$ ion density promotes denser films denser thanks to enhancement of ion bombardment. However, most of the time, the deposition rate is weakly affected and the crystalline quality of the film tends to decrease and even change to an amorphous structure[31,32]. On the contrary, the increase of $Cr^+$ ion density usually improves the conformity and crystalline quality of the deposited films[33,34]. In addition, the metallic ions directly contribute to the film growth.

In the present paper, we present the effect of synchronized additional pulses applied at different time of the main HiPIMS pulse on both the discharge composition and the quality of deposited films in the case of pure Cr films.

## II. Experimental details

The HiPIMS measurements and films depositions were performed in a cylindrical stainless-steel chamber where the cathode is located vertically above the sample holder, which can be polarized to control the energy of ions impinging the substrate surface. Thanks to a turbo molecular pumping unit from Leybold, a background pressure close to $3.10^{-4}$ Pa can be achieved. Two capacitance and ionization gauges allow to follow the deposition pressure and the background pressure, respectively. The size of magnetron target is a disc of 7.6 cm diameter.

Since the rotational speed of the turbo molecular pump remains constant, the working pressure is manually controlled by a regulation valve between the deposition chamber and the pumping system (Leybold). The gas is introduced via a mass flowmeter (Brooks®) and and the gas flux is monitored by a computer interface.

To analyze the discharge, and in particular the evolution of electrons population versus time, we performed electrical characterization of the discharge by a commercial Langmuir probe measurements (using a commercial probe from Impedans [35]). A single tungsten tip (10 mm length and 0.195 mm radius) in the standard configuration was used to probe the plasma out of the ionization region (magnetized plasma).

The probe tip is connected to RF and DC compensation electrodes to increase the capacitive coupling between the probe tip and the plasma and to compensate for the perturbation of the plasma potential caused by the probe biasing. Temporal analysis of plasma is possible because the Langmuir probe operates at an 80 MHz sampling rate, which allows a plasma diagnostic every 12.5 ns. This enables a very good time resolution for HiPIMS pulses as short as a few tens of μs.

This probe has very good performances in terms of the plasma potential range (-100 V to +145 V), the ion current density (1 μA/cm$^2$ to 300 mA/cm$^2$), and the electron temperature (0.1 eV to 15 eV). Out of the magnetic trap, the probe was placed 5 cm away from the cathode. The radial displacement of the probe permits the radial measurements of current-voltage (I-V) characteristics. Here we fixed the radial position in front of the racetrack. Plasma parameters such as the electron temperature, electron density, plasma potential and floating potential can be easily extracted from the I-V characteristics. The ion mean free path is large for low

pressures, and the sheath around the probe is assumed to be collisionless. Thus, the probe current is determined by the Laframboise orbital motion theory.[36] Therefore, all these plasma parameters are automatically evaluated using the Impedans software.[35]

A typical HiPIMS pulse comprises two phases: the time-on and the time-off. The time-on, $t_{on}$, corresponds to applying a high negative voltage (about 500-700 V in absolute value) to the cathode during tens of microseconds. The time-off, $t_{off}$, corresponds to the cut-off of the high voltage applied to the cathode between two successive pulses. In the latter phase, a progressive extinction of the plasma is observed. These two phases are repeated with a period T.

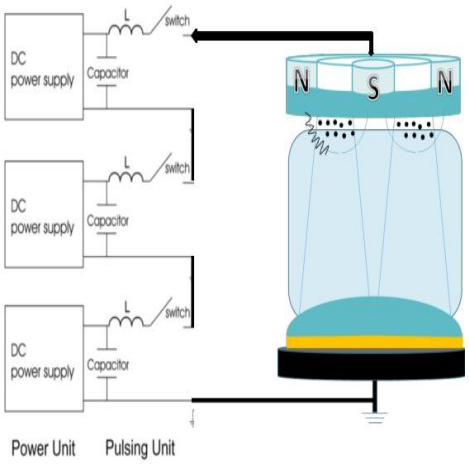


**Figure 1. Simplified scheme of the e-HiPIMS power supply that displays LC circuits.**

In our previous study,[21] , we showed that two regimes exist during the same HiPIMS Ar/Cr discharge pulse. The first one characterizes the beginning of the pulse, in which $Ar^+$ dominates. This is the period when the current rises and the gas atoms get massively ionized, but the Cr atom sputtering stays deficient. The second regime is $Cr^+$ dominated, due to the argon rarefaction that increases the relative number of Cr atoms in the ionization region. Therefore, their ionization is enhanced due to the higher direct collision probability with the trapped electrons and their lower ionization energy than argon.

In this study, we propose adding an extra short-voltage pulse at the beginning of the regime dominated by the $Cr^+$ ions. Hence, it should boost the ionization process of Cr by electron impact and amplify the $Cr^+$ production.

Therefore, the experiments were carried out using the e-HiPIMS power supply. It comprises three LC circuits (three stages, Fig. 1) operating repetitively and synchronized. In addition,

each stage can be turned on or off, and can deliver a negative voltage between 150 and 300 V. This means that during a pulse sequence, each stage can deliver a square voltage signal with a specific duration $t_{on}$, and with a specific delay with respect to the beginning of the sequence. Hence, the operation mode can be standard HiPIMS (s-HiPIMS) when all the stages deliver the voltage simultaneously (no delay between the stages) or multi-voltage pulse sequence m-HiPIMS when the stages are shifted in time.[25,27]

A homemade software manages each voltage stage in the desired sequence (amplitude, width, delay, etc.). The voltage pulse value is a set point, meaning the cathode applied value can differ slightly from the imposed reference. For example, if the set point value is 700 V, the applied value would be 700 ± 20 V.

Figure 2 shows, for the sake of example, three multi-voltage pulse sequences produced by the new power supply. Each configuration comprises a main voltage stage of 500 V between 0 and 30 µs (the orange section) and an additional voltage stage of 200 V (the blue section). Standard HiPIMS (D1, Fig. 2) is the addition of these two stages (700 V). For $D_2$, the first stage is 500 V between 0 and 25 µs, 700 V between 25 and 30 µs, and 200 V between 30 and 40 µs. This sequence aims to favor the $Cr^+$ production. For D3, two additional voltage stages are added at different intervals. The first is between 5 and 15 µs to favor $Ar^+$ production and help Cr sputtering. The second one is added between 20 and 40 µs to favor $Cr^+$ production. Table 1 summarizes the three configurations with associated discharge voltages. These three configurations $D_i$ (i=1-3) are discussed in the present study.

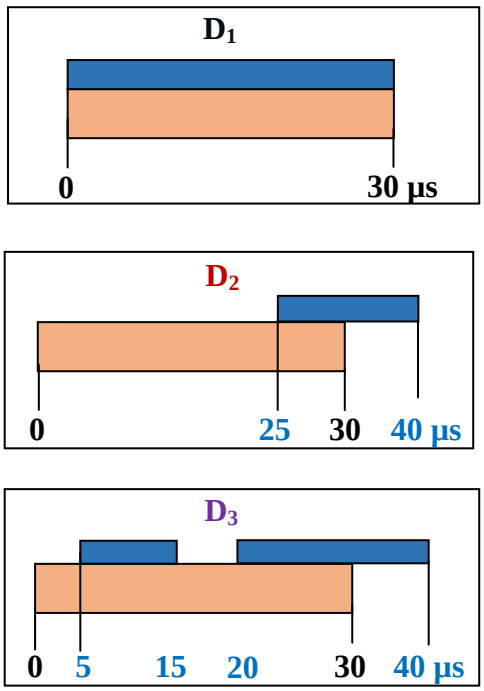

**Figure 2. The three configurations of pulse sequences ($D_1$, $D_2$, and $D_3$) obtained with the new pulsed power supply. They are compared hereafter.**

**Table 1: Voltage values for each configuration during $t_{on}$. Notice that all the voltage values are negative but indicated in absolute value for convenience. Red values indicate the addition of the voltage delivered by at least two stages of the power supply, while blue values the remaining voltage from one single stage after the cut-off of the main stage. The black values indicate the voltage of the main stage.**

| $t_{on}$ (µs) | 0 - 5 | 5 - 15 | 15 - 20 | 20 - 25 | 25 - 30 | 30 - 40 |
|---|---|---|---|---|---|---|
| Voltage - $D_1$ ≈ | **700** V | **700** V | **700** V | **700** V | **700** V | 0 V |
| Voltage - $D_2$ ≈ | 500 V | 500 V | 500 V | 500 V | **700** V | **200** V |
| Voltage - $D_3$ ≈ | 500 V | **700** V | 500 V | **700** V | **700** V | **200** V |

Figures 3, 4 and 5 present the measured voltage and current waveforms of the three pulse sequences $D_1$, $D_2$ and $D_3$ (detailed in Fig. 2 and Table 1), respectively. In all cases, a transient regime is observed before reaching a constant voltage (steady state). The experiments were performed for a pressure of 0.6 Pa and an average power of around 200 W.

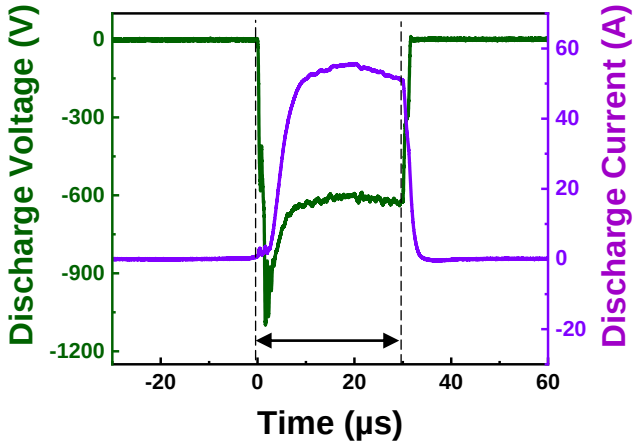


**Figure 3. Typical current and voltage waveforms for $D_1$ (s-HiPIMS).**

For different $D_i$ (i = 1-3), a delay between the current and the voltage is observed at the beginning of the pulse. This delay corresponds to the ionization time to build up the ion ($Ar^+$) space charge, mainly in the ionization region (IR), and the gas ions' flight time across the

sheath between the IR and the cathode. Once the $Ar^+$ hits the target, a significant amount of metal atoms leaves the target. After a few µs (typical flight time), they reach the IR. After that, the ionization of sputtered metal (Cr) leads to a significant production of $Cr^+$ and $Cr^{++}$, contributing to the increase of the total discharge current.[37] Notice that the amount of metal ions increases, and the self-sputtering can also increase.

For $D_1$, the voltage and the current behavior during $t_{on}$, from 0 to 30 µs, are as expected, typical for the s-HiPIMS. The voltage slightly decreases at the beginning of the pulse due to the current rise and the voltage drop on the internal exit resistance of the pulsing unit. When the current stabilizes, the discharge voltage reaches a stable value of 600 V. During $t_{on}$; the current reaches a maximum of 50 A (1.13 A/cm$^2$). After this maximum, the total current slightly decreases, which is the typical behavior of the HiPIMS plasma operated with a chromium target.

One explanation is the replacement of a significant fraction of the gas ions by metal ions (single and multiple-charged). After 30 µs, the voltage switches off to zero. Consequently, the discharge current abruptly decreases.

For configuration $D_2$, the sequence starts with a high voltage pulse, like in the previous sequence, with the same duration of 30 µs. In $D_2$, a voltage over-pulse of 200V adds power to the discharge starting at 25µs. This additional pulse ends beyond the end of the starting pulse at 40 µs. As Figure 4 illustrates, the current and the voltage evolution shows three different levels: $L_1$, $L_2$ and $L_3$, since the voltage changes during all three phases (see Table 1 and Fig. 2).

At the beginning of the pulse from 0 to 25 µs (level $L_1$), the initial voltage (~ 900 V, Fig. 4) decreases to about 500V, towards a plateau. Then the voltage jumps to the $L_2$ level, around 700 V, due to the over-pulse (additional ~200V). Due to this short added voltage on the cathode, the steady state of nearly constant voltage does not occur. Finally, when the first pulse of the sequence is cut off (30 µs), the transition from $L_2$ to $L_3$ marks a significant voltage drop, close to zero, before entering phase $L_3$. During $L_3$, from 30 to 40 µs, the voltage gradually increases to reach the reference operation point of about 200 V. Still, no steady state can be reached since the plasma evolves in a transitory regime.

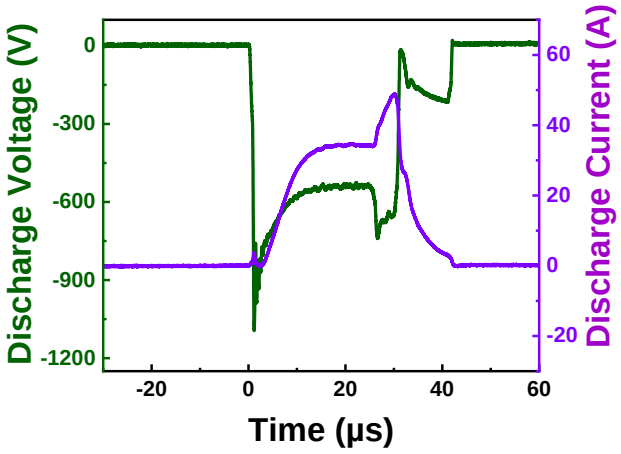


**Figure 4. Current and voltage waveforms for the pulse sequence $D_2$. Labels $L_i$ (i = 1,3) indicate the time intervals with different voltage levels summarized in Table 1.**

Let us analyze the current evolution (Fig. 4, right Y-axis). Let us emphasize the difference between D2 and the reference sequence D1; after 30 μs, the current immediately decreases for D1 and gently decreases for D2. During the L1 of D2, the current has a similar behavior as recorded in sequence D1. So, from 0 to 25 μs, the current increases at around 30 A, much less than in D1 (peak current ~50A) due to the voltage reference level set to ~700V in D1 but only 500V in L1 of D2. Then, after adding the extra voltage pulse at level L2 (from 25 to 30 μs), the current reaches a maximum of 45 A (close to the peak value in D1). At level L3, the current continuously decreases when the voltage decreases from 700 to 200 V. This is highly expected because only 200V supports the discharge. After 40 μs, there is neither voltage nor current when the pulse sequence D2 is fully off. This behavior of $D_2$ is also observed for $D_3$, as discussed below.

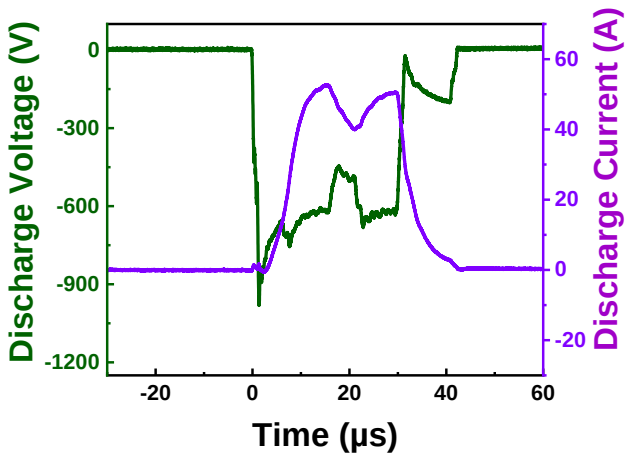


**Figure 5. Current and voltage waveforms for the pulse sequence $D_3$. Labels $L_i$ (i = 1,5) indicate the time intervals with different voltage levels summarized in Table 1.**

For configuration $D_3$ (Fig. 5), the sequence starts with a high voltage pulse (called the original pulse since it marks the beginning of the sequence), like in the previous sequence ($D_1$ and $D_2$, ~ 900V at the beginning), with the same duration of 30 µs. Two additional voltage pulses (or over-pulses) are superposed to the first with different durations and delays. The first adds ~200V for a very short time, between 5 and 15 µs. When this first over-pulse switches off, the original of 30 µs is not finished, and 5 µs after, a second over-pulse adds again ~200V, between 20 and 30 µs.

Let us now analyze the voltage and current evolutions for the $D_3$ sequence (Fig.5) with respect to $D_2$. At the beginning of the pulse from 0 to 5 µs (level $L_1$), the voltage should normally reach 500V. This voltage level is close to the transient value observed in the previous sequences D1 or D2 exactly after 5 µs from the beginning of the pulse. However, since the time interval is very short, the steady state is not reached, and the voltage is higher than the expected set point.

Then at $L_2$, after adding the first over-pulse (~5 µs), the voltage slightly increases, followed by a decay around 700V. The voltage level starts to stabilize in the second half of this first over-pulse (between 10 at 15 µs). However, the steady state does not survive because phase $L_3$ begins. This level of $L_3$ is very short (~5 µs length), between 15 to 20 µs. During $L_3$, the voltage drops from 700 V to 500 V. Then, the second over-pulse starts at 20 µs. Up to 30 µs, a new level of $L_4$ is attained. The voltage reaches 700 V again, very fast. Further, during the transition from $L_4$ to $L_5$, the voltage drops to a low value close to zero (like in sequence $D_2$) before entering the $L_5$ phase. In $L_5$, which lies from 30 to 40 µs, the voltage increases to around 200 V without reaching a steady state.

Let us comment on the current evolution (Fig. 5, right Y-axis). The discharge current keeps increasing during levels $L_1$ and $L_2$, from 0 to 15 µs, without observing any transition until reaching a maximum value of 50 A. Notice this peak value is the same as for s-HiPIMS ($D_1$), but in $D_3$, the maximum is reached faster, after only 15µs, while in $D_1$, the current peaks after about 20 µs (Fig. 3). In the following, the current decays because of the voltage set point decreases from 700 ($L_2$) to 500 V ($L_3$). At $L_4$, the second over-pulse brings additional power to the discharge, and the current increases again until around 45 A, below the peak value (recorded in $L_2$). As in $D_2$, for level $L_5$, the current decreases continuously and smoothly due to the abrupt voltage drop from 700 to 200 V.

Figure 6 shows the influence of the pressure, for 0.2, 0.6, and 1 Pa, on the current waveform for the three pulse sequences $D_1$, $D_2$, and $D_3$. The current increases with the pressure independent of how the power is delivered to the plasma. The fingerprint of the current stays similar for the three studied pressures, and the signature of specific levels discussed above characterizes each pulse sequence. However, at the pulse's beginning, the delay between the voltage and the current decreases while the pressure increases, as expected. The higher the pressure, the faster the space charge builds up.

For all studied configurations, the observed delay of around 1 to 5µs decreases by increasing the pressure, at constant applied voltage. As previously studied30, this delay is also linked to the applied voltage.

Indeed, the delay is related to the ionization time necessary to the discharge to create enough electrons and ions and the time for the primary electrons (ejected from the target) to get accelerated in the sheath electric field, between IR and the cathode.[34,35] Let us consider the following approximation to evaluate the ionization time's dependence on the pressure. The ionization time ($\tau_{ionization}$) is related to the argon density ($n_{Ar}$) and the argon ionization rate, which depends on the electron temperature $T_e$. This can be expressed as:

$$\tau_{ionization} = \frac{1}{n_{Ar} \times K_{ionization}(T_e)} \quad (1)$$

At the beginning of the voltage sequence, time-on $T_e$ is around 6 – 8 eV (previously calculated in our HiPIMS model[38]), $n_{Ar}$ is proportional to the pressure:

$$n_{Ar} = \frac{P}{K_B\, T} \quad (2)$$

$K_B$ is the Boltzmann constant and $T$ is the gas temperature (300 K). This is particularly true in the early stages of the pulse when the gas rarefaction is not yet active. Moreover, $K_{ionization}(T_e)$ of argon is calculated as[38] :

$$K_{ionization}(T_e) = 1.17 \times 10^{-7}\, e^{\frac{-21.7}{T_e}} \quad (3)$$

Therefore, for $T_e$ equal to 6.5 eV and pressure of 0.2 Pa, 0.6 Pa and 1 Pa $\tau_{ionization}$ equals 5 µs, 1.7 µs, and 1 µs, respectively. P. Poolcharuansin and J.W. Bradley[39] have measured between 0 and 4µs, three distinct groups of electrons with effective temperatures of 70–100 eV, 5–7 eV and 0.8–1 eV. After ~ 4 µs, it remains only a single distribution with an electron

temperature of about 5 eV. It means that our mean electron temperature estimated at 6.5 eV is consistent with these measurements.

As explained by G.Y. Yushkov and A. Anders,[30] the delay time is close to the time required for the discharge to develop using the primary electrons, corresponding to the ionization time (Eq. (1), see also Fig. 6-a). Hence, by increasing the pressure, the ionization time of atoms decreases. For low pressure, electron-atom collisions are scarcer, reducing the frequency of the ionization events. Consequently, the delay between the applied voltage and current growth becomes more significant. Remember that all previously reported results have been obtained for an average power of 200 W on the cathode. Hereafter the power is 100 W for the following experiments. First, the current and voltage were measured for different conditions. For configuration $D_1$, the current peaks to 18 A (at 0.2 Pa) when the voltage pulse is on and decreases immediately at 30 µs when the discharge is off.

Therefore, the current delay with respect to the voltage is ~5 µs for 0.2 Pa. Meanwhile, it occurs at 2 and 1 µs for 0.6 Pa and 1 Pa, respectively. Table 2 shows the voltage set point and peak current values for each pulse sequence at different periods during the sequence for the three studied argon pressures, namely 0.2, 0.6 and 1 Pa.

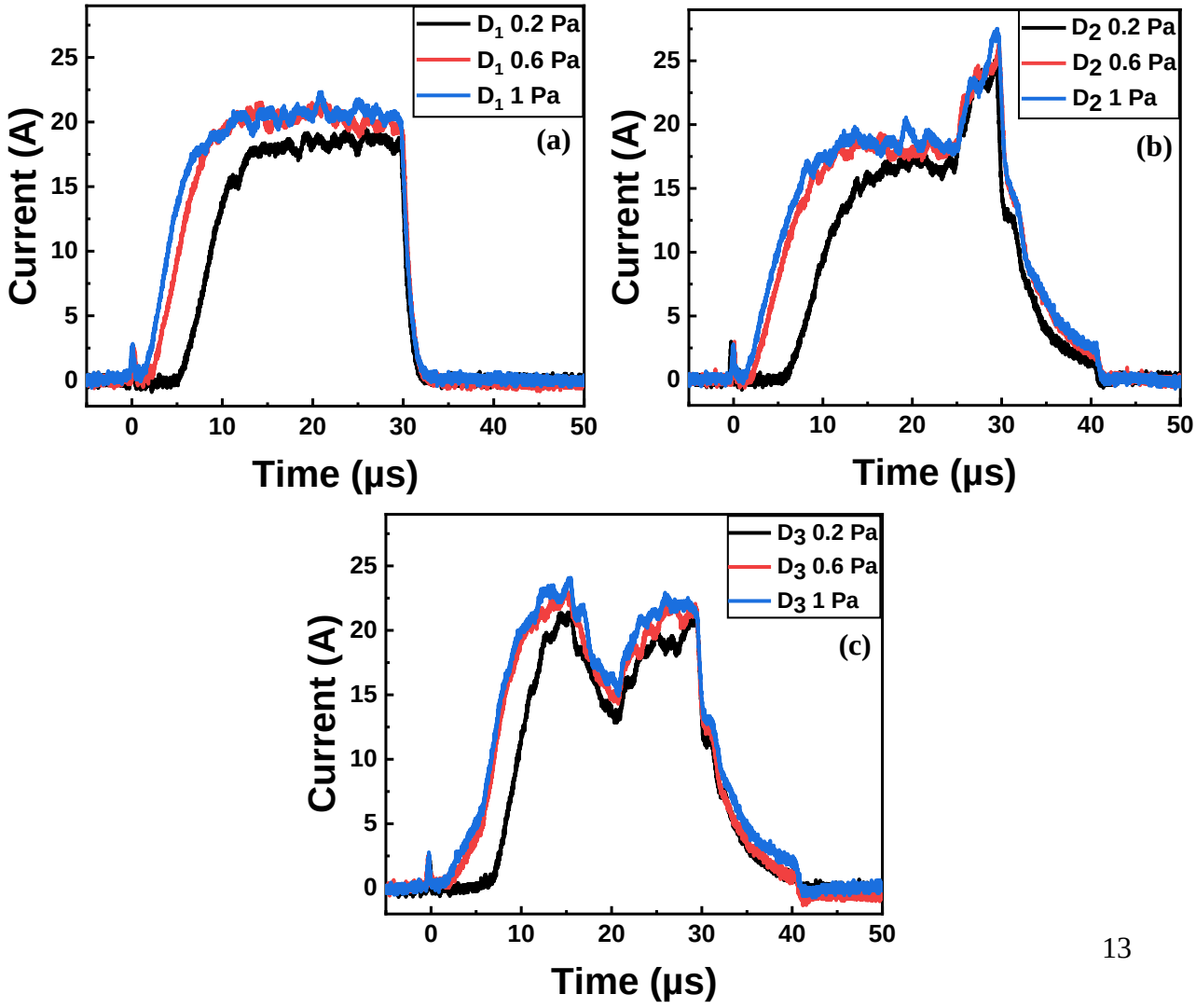

**Figure 6. The evolution of the discharge current for three pulse sequences (a) $D_1$, (b) $D_2$ and (c) $D_3$ (detailed in Table 1 and Fig. 2) for three argon pressures of 0.2, 0.6, and 1 Pa.**

For configuration $D_2$ at level $L_1$ (between 0 and 25 µs), the current increases to 15 A for 0.2 Pa and 17 A for 0.6 Pa and 1 Pa. During $L_2$, when the voltage over-pulse is added between 25 and 30 µs, the current peaks at 22 A for 0.2 Pa and 0.6 Pa and about 25 A for 1 Pa. After that, during phase $L_3$ (between 30 and 40 µs with 200 V), the current slightly decreases, following practically the same path, independent of the working pressure. However, at 1 Pa, there is a slight overshot (increase) of the current before starting the last level of this sequence, absent for the other pressures. This could be attributed to the enhanced ionization of Ar.

**Table 2: The current peak and voltage values for each pulse sequence during different time intervals of the $t_{on}$ for the same average power of 100 W and three working pressures of 0.2, 0.6, and 1 Pa of argon.**

| | $D_1$ 10-30 µs | $D_2$ 10-15 µs | $D_2$ 25-30 µs | $D_3$ 10-15 µs | $D_3$ 25-30 µs |
|---|---|---|---|---|---|
| | 700 V | 500 V | 700 V | 700 V | 700 V |
| 0.2 Pa | 17 A | 15 A | 22 A | 20 A | 18 A |
| 0.6 Pa | 18 A | 17 A | 22 A | 22 A | 20 A |
| 1 Pa | 18 A | 17 A | 25 A | 23 A | 20 A |

Similar behavior appears for $D_3$. For low pressure of 0.2 Pa, the delay between the current and voltage slightly exceeds 5 µs. When the first voltage over-pulse starts, during $L_2$ between 5 and 15 µs, the current peaks to its maximum for the three pressures. These maxima slightly increase with the pressure. Then the current decreases by 2/3 between 15 and 20 µs (level $L_3$) when the voltage also decreases. After that, the second voltage over-pulse starts (corresponding to $L_4$ from 20 to 30 µs). The voltage has the same level as in $L_2$, but the current increases less and reaches a value below the maximum (in $L_2$). This current limitation could be attributed to the intensification of the gas rarefaction phenomenon in the ionization region, inducing a decrease in the ionization rate and, therefore, a decrease in the discharge current.[38] Then, at $L_5$, between 30 and 40 µs, a sharp current decay occurs.

In this part, it is established that using an over-pulse enhances the total current. The over-pulse creates hot electrons that ionize the species present in the IR. Naturally, when the

pressure increases, the density of these species increases as well, and consequently, the total charge carried by the discharge (table 3).

**Table 3: Integration of the current for each pulse in Coulomb sequence (same average power of 100 W) and three working pressures of 0.2, 0.6, and 1 Pa of argon.**

| | $D_1$ | $D_2$ | $D_3$ |
|---|---|---|---|
| 0.2 Pa | 381 C | 415 C | 416 C |
| 0.6 Pa | 503 C | 544 C | 538 C |
| 1 Pa | 537 C | 563 C | 547 C |

## III. Langmuir probe results

Langmuir probe measurements were carried out to obtain time resolved electron density and temperature. The Langmuir probe was outside the ionization region (IR), characterized by a very high electron density $n_e$. Note that the IR is located a few millimeters from the cathode and typically expands about 2 cm. The probe location (8 cm from the target) was far enough from the magnetic trap, so one can assume there is no magnetic field effect on the probe signal. The results presented hereafter do not consider any correction due to the magnetic field. The measured values of $n_e$ and $T_e$ outside of the IR are obviously different from those in the IR.[37]

Figure 7 shows the electron density and temperature evolution during the pulse and the beginning of the afterglow of all three studied pulse sequences $D_i$ (i=1-3) at low pressure, 0.2 Pa. When the discharge is 'on', the electron density increases until it reaches a maximum value around $(2.8 \pm 0.5)\times10^{16}$ $m^{-3}$, $(1.2 \pm 0.5)\times10^{17}$ $m^{-3}$, and $(1.3 \pm 0.5)\times10^{17}$ $m^{-3}$ for $D_1$, $D_2$ and $D_3$, respectively. Noting that at the beginning of the discharge, $D_1$ starts with a voltage of 700V, while $D_2$ and $D_3$ start with 500V each. During the pulse sequence, the electron density increases continuously until reaching a maximum, about 35 µs after the start of the sequence, independent of the way the power is delivered to the discharge. Then the electron density decreases, surviving even 100µs after the end of the pulse when it is typically one decade lower. In addition, the electron density correlates well with the pulse sequence voltage level. $D_3$ has the highest electron density, followed by $D_2$ and $D_1$. Notice, however, that the difference between $D_3$ and $D_2$ is in the margin of the error bar. This means that the effect of

the over-pulse on the diffusion plasma keeps less the memory of the moment when it is applied but depends significantly on the voltage level.

In $D_3$, the first voltage over-pulse starts only 5 µs after the beginning of the sequence (up to 15 µs), reaching around 700 V. The electron density rises fast and reaches a first maximum of $9.4 \pm 0.5 \times 10^{16}$ $m^{-3}$ at the end of this over-pulse (~15 µs), then decreases when the voltage also decreases (down to 500V in L3). The second voltage over-pulse starts at 20 µs (up to 40 µs). The electron density peaks at $1.3 \pm 0.5 \times 10^{17}$ $m^{-3}$ at around 35 µs. Notice that at this moment, the voltage is only 200V since the original pulse lies 30µs. However, the probe's position is out of the IR, and it captures the density value in the diffusion plasma. Is expected a delay between the maximum value in the IR (not measured, but expected to be in phase with the injected power, which is maximum in $L_4$) and at the location of the probe.

Comparing the electron density augmentation between $D_2$ and $D_3$ with respect to reference $D_1$ unveils the influence of the over-pulses on plasma. For $D_3$, the electron density increases between 5 and 15 µs, followed by a second boost between 27 and 37 µs.

Hence, at least in front of the substrate, the electron density is higher when a second voltage over-pulse is added around the middle of the discharge. The first observed electron density peak is assigned mainly to the Ar ionization process. The second one mainly produces metal ionization, enhancing the density of $Cr^+$ and $Cr^{++}$. They were also observed and discussed by Poolcharuansin and Bradley.[39] The effect of the second peak on the electron density is higher than the first one due to the lower ionization energy threshold of Cr (7.68 eV) compared to Ar (15.76 eV). After reaching the maximum, the electron density decreases because the power decreases.

For similar conditions, other studies observed an electron density of $10^{18}$-$10^{19}$ $m^{-3}$. On the other hand, in our study, the electron density is around $10^{17}$ $m^{-3}$. This is due to the placement of the Langmuir probe, which is not in the ionization region (magnetized trap) where the density is expected to be at least one order of magnitude higher; it is placed at 8cm (close to the substrate position) and perpendicular to the target. Thus, some of the electrons could eventually not be detected, which could affect the electron density [40,41]. Therefore, the apparent electron density is lower than what has been observed for the case of HiPIMS in other studies.

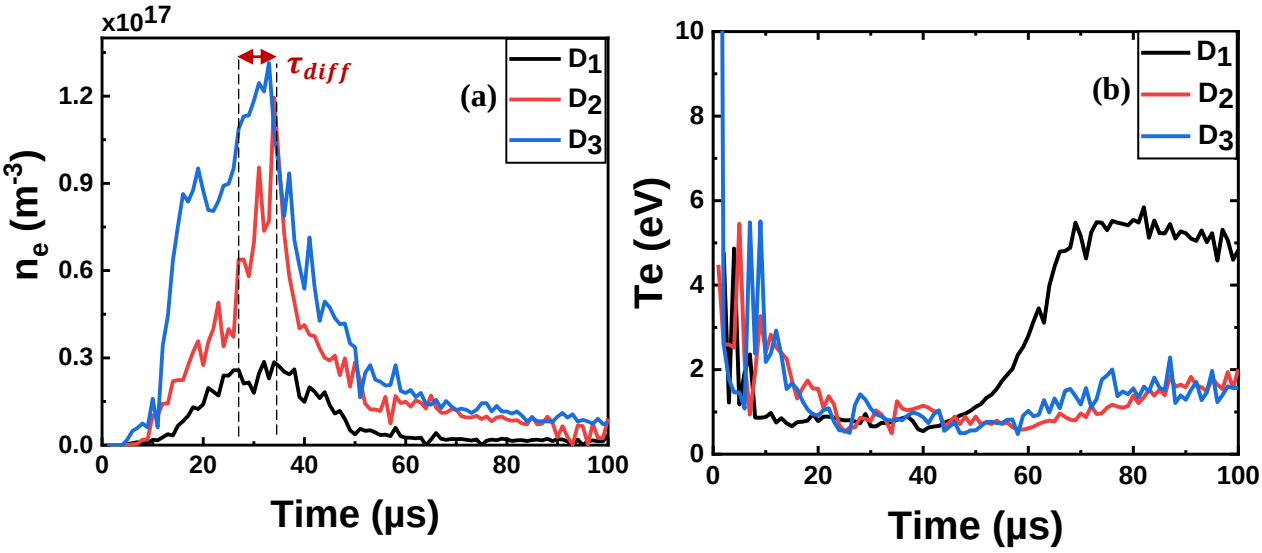


**Figure 7. Time evolution of the electron density (a) and electron temperature (b) for the three pulse sequences in Table 2 and argon pressure of 0.2 Pa.**

Furthermore, one can see a striking difference between the $n_e$ peaks' shape (Fig. 7) and the currents' evolution (Fig. 6). The current is measured on the cathode, which is very close to the IR. In contrast, the $n_e$ is measured by the Langmuir probe, which is located 5 cm away from the cathode. For example, the two current peaks are associated with the two voltage over-pulses of the $D_3$ sequence and registered in the time intervals 5-15 μs and 20-30 μs. They are less obvious but still present in the time profile of $n_e$. The overlapping of the peaks in the case of $n_e$ could be attributed to the electron diffusion phenomenon from IR towards the Langmuir probe.

The diffusion results in an enlargement (dispersion) of peaks in time, inducing an overlapping of the two (close) successive peaks.

The electron density increases when the power injected in the plasma increases by applying the additional over-pulse. For the D2 sequence, the voltage over-pulse starts at 25 μs and finishes at 40 μs. Hence, the electron population is less spread than in D3 at the discharge's beginning, but the density level is also lower. The time shift between the maxima values of recorded electron density and current (Fig.6) is about 8 μs, which could correspond to the ionization enhancement and electron diffusion out of the IR to the Langmuir probe.

In fact, in first approximation, the average diffusion time of electrons writes:

$$\tau_{diff} = \frac{L^2}{D_e} \qquad (4)$$

Where $L$ is the distance between IR and Langmuir probe, and $D_e$ is the Bohm diffusion coefficient of electrons. The probe is placed outside the magnetized zone. Hence, the Bohm diffusion is important because inside IR, it delays the electron's diffusion, and outside IR, it neglects the diffusion time. Notice also that most ionization events occur within a few millimeters in front of the racetrack.[40] So, it is reasonable to assume $L \cong 8\,cm$. For $\tau_{diff} = 7 - 8\,\mu s$ , $D_e = 4.2 \times 10^6\,cm^2/s$. This value for $D_e$ is in good agreement with the value reported in REF[38] for our pressure range.

Let us look at the evolution of the electron energy, namely electron temperature (Fig. 7(b)), given by Langmuir probe measurements. By disregarding the strong noise, the evolution of $T_e$ as a function of time shows a sharp increase at the beginning of time-on, followed by a decay (relaxation) until the end of the sequence at 40 µs. In the afterglow, between 40 and 80 µs, $T_e$ increases again for $D_1$, while for $D_2$ and $D_3$, only a weak increase is observed. Beyond 80 µs, $T_e$ unconditionally decreases.

The electron temperature evolution in the afterglow is related to the recombination kinetics. Indeed, low-energy electrons attach first, letting free only a fraction of energetic electrons. On the other hand, non-magnetized electrons diffuse faster to the wall, and the positive space charge dominates the afterglow plasma. Hence, the surviving free electrons have higher energy than during the plasma pulse, but their density is drastically reduced.

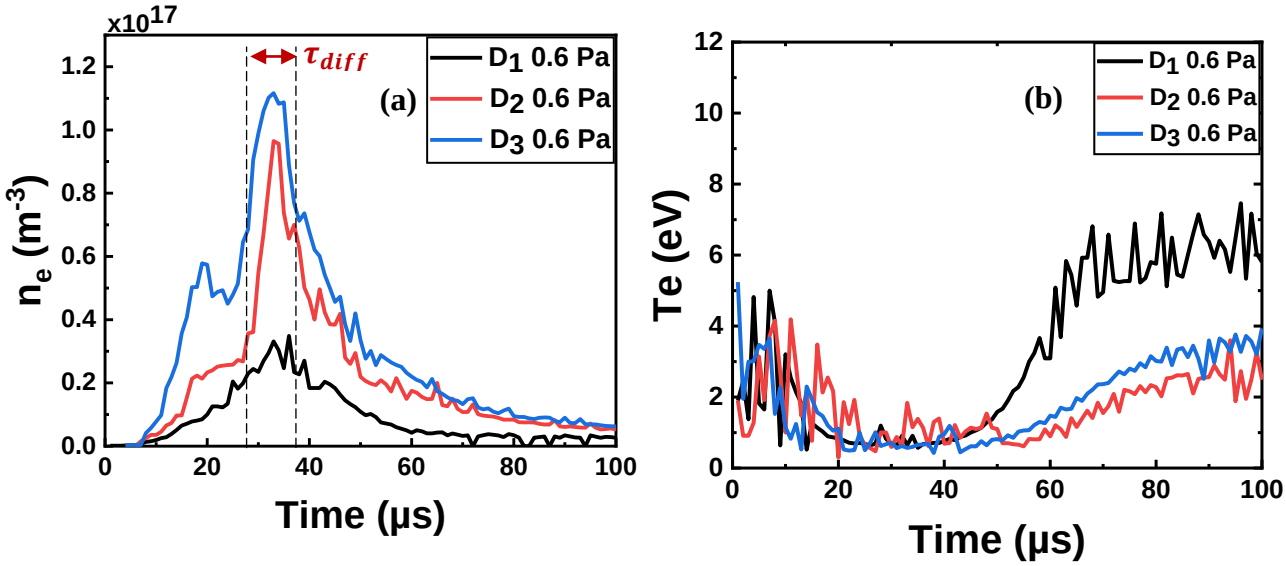

**Figure 8. Time evolution of the electron density (a) and electron temperature (b) for the three pulse sequences in Table 2 and argon pressure of 0.6 Pa.**

Figure 8 presents the electron density and temperature of all configurations $D_i$ (i=1,3) for 0.6 Pa pressure. The average power was fixed at 100 W. The electron density behavior is similar to the evolution observed at lower pressure, 0.2 Pa (Fig. 7). At the beginning of the pulse, the electron density increases. Then it reaches a maximum value of $(3.5 \pm 0.5)\times10^{16}$ $m^{-3}$, $(9.6 \pm 0.5) \times10^{16}$ $m^{-3}$, and $(1.2 \pm 0.5) \times10^{17}$ $m^{-3}$ for $D_1$, $D_2$ and $D_3$, respectively. During time-on, $n_e$ is higher for $D_3$ than for $D_1$ and $D_2$. Adding the voltage over-pulses in $D_2$ and $D_3$ increases the electron density compared to $D_1$. This could be explained by the fact that at high pressure, the Cr thermalization is faster; hence, the ionization during the additional pulse becomes more efficient for $D_2$ and $D_3$. In the afterglow (time-off phase), the electron density smoothly decays for all of the configurations.

The electron temperature has a very similar behavior when the pressure increases from 0.2 (Fig. 7(b)) to 0.6 Pa (Fig. 8(b)). It is about 4 ± 0.5 eV for all sequences at the beginning of time-on and continuously decays to about 1 eV until the end of the sequence. In the afterglow, it rises again (see the explanations above). However, for both $D_2$ and $D_3$, the rise of the electron temperature at regular intervals is less pronounced at higher pressure, but it does occur.

Figure 9 shows the electron density of each configuration $D_i$ for 0.2 Pa and 0.6 Pa pressures. The maximum of $n_e$ is outside of the time-on. As said, this shift is due to the diffusion time of the electrons from IR towards the Langmuir probe (see Eq. 4).

For $D_1$, at first, $n_e$ decreases with the pressure increase. This decrease could be due to the slight cooling of the electrons induced by the higher collision frequency (higher pressure). About the afterglow, $n_e$ survives longer at higher pressure beyond the end of the pulse because the density at the end of the pulse is higher. This could be explained by the decrease of the rarefaction phenomenon of Ar gas, which tends to increase the partial pressure of Ar and consequently increase the electron production rate by the ionization process. Also, as discussed in Gudmundsson *et al*. study [42], the argon metastable can also play an important role with the pressure increase. However, the influence of the pressure less affects sequence $D_2$ than $D_3$.

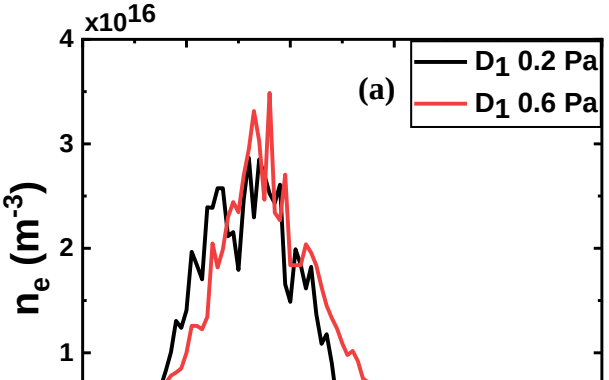

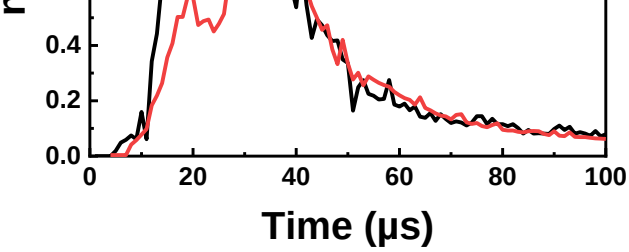


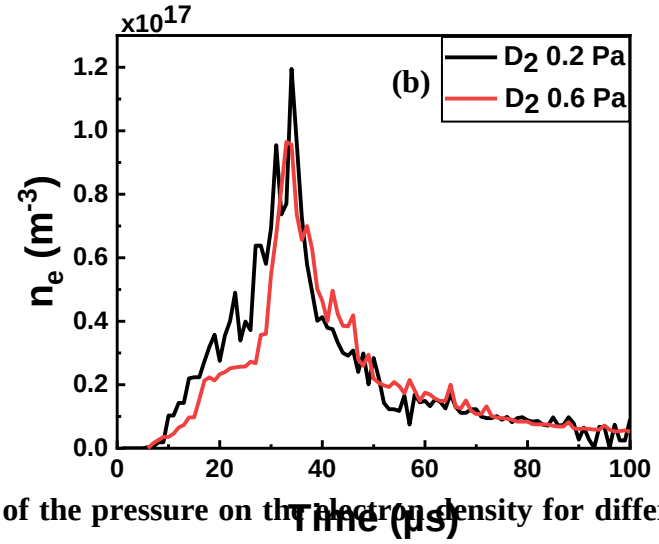


**Figure 9. Influence of the pressure on the electron density for different pulse sequences (a) $D_1$, (b) $D_2$ and (c) $D_3$ given in Table 2.**

For all sequences, the electron density is higher at the end of the pulse at higher pressure. Even when the second voltage over-pulse is applied, the electron density stays higher for low pressure (0.2 Pa). This is because the ionizations occur in the IR, but their diffusion is highly limited with the pressure increase. For D3, when the first over-pulse is added between 5 and 15 µs, the electron density rises less by increasing the pressure to 0.6 Pa.

Figure 10 shows the electron temperature of each configuration for the same two pressures, 0.2 Pa and 0.6 Pa. Disregarding the noise generated during the measurement of $T_e$; globally, $T_e$ increases with the pressure whatever the HiPIMS sequence $D_i$ (i=1,3) is.

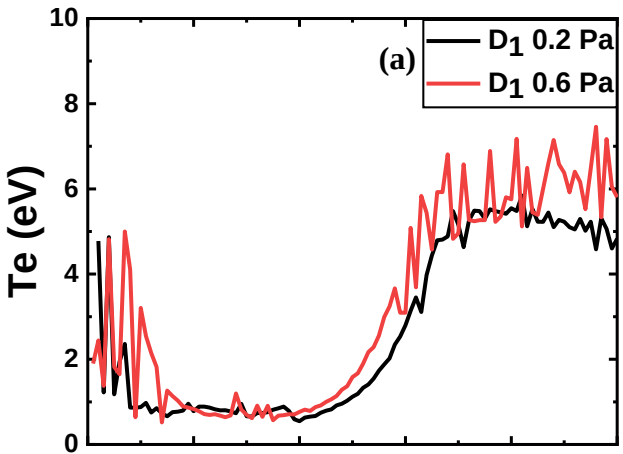

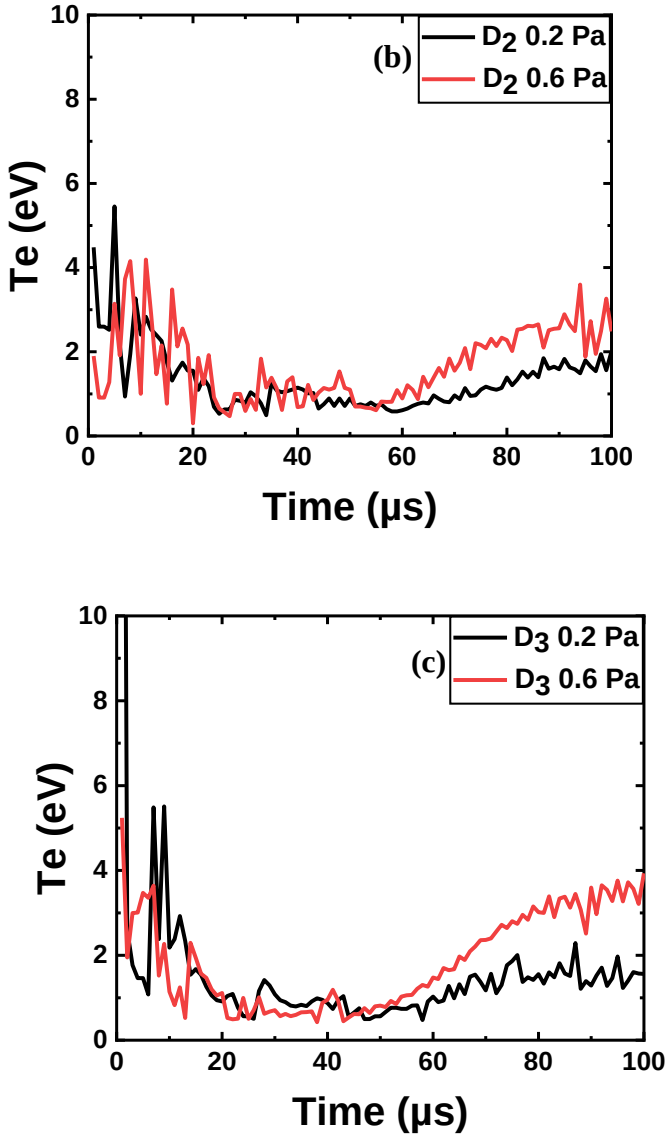


**Figure 10. Influence of the pressure on the electron temperature for different pulse sequences (a) $D_1$, (b) $D_2$ and (c) $D_3$ given in Table 2.**

## IV. CONCLUSION

In this paper, we investigated a prototype of e-HiPIMS power supply, neither studied nor published before. We characterized the effect of such power supply on the generated plasma characteristics. The advantage of such supply lies in the possibility to generate independently multi-pulses and to synchronize a main pulse with one or several over-pulses at chosen moments during the time-on of the main pulse with an independent delay and duration. Thus, specific ion populations can be amplified by well-chosen over-pulses.

Win the present study, we compared three different pulse sequences; thereafter called $D_1$, $D_2$ and $D_3$. The first sequence $D_1$ stands as the reference and corresponds to a conventional HiPIMS power supply behaving like the standard HiPIMS (s-HiPIMS).

The second sequence, $D_2$, has an additional voltage over-pulse between 25 and 40 µs of the main pulse, aiming at amplifying the chromium ionization by the end of the pulse. For the third sequence, $D_3$, two voltage over-pulses have been added: a the first one between 5 and 15 µs of the main pulse, aiming at amplifying the argon ion density and thus increase the target sputtering, going along with bringing more Cr atoms into the plasma phase, while the second one applied between 20 and 30 µs is expected to boosts the chromium ionization. Time-resolved measurements by the Langmuir probe gave allowed to collect supplementary information on electron density and temperature evolution.

The pressure and power changes revealed their influence on each pulse sequence. As a result, we found that sequence $D_3$ provides the highest electron density during the discharge. Then, $D_2$ has the second highest electron density. Note that when the voltage over-pulse is added, the sequence has the same total voltage as in $D_1$ (s-HiPIMS). For $D_3$, the increase of $n_e$ with the pressure is remarkable because of the addition of two voltage over-pulses. However, when the pressure increases, the electron density decreases for an average power fixed at 100 W.

Meanwhile, the electron temperature presents different behaviors: at the beginning of the pulse, the temperature is high and decreases in a second time to further to increase at the beginning of the afterglow (time-off). The electron temperature increases again when the following over-pulse is added.

Such results have thus shown their interest with respect to the standard HiPIMS. The e-HiPIMS offers a higher flexibility by adding one or several over-pulses at well-chosen moments in the main pulse with tunable duration in addition to the typical s-HiPIMS parameters, i.e. the pulse width and the frequency in s-HiPIMS.

Thus, this novel e-HiPIMS power supply allows a better control of the HiPIMS deposition process. Our study has shown the possibility of amplifying the HiPIMS discharge current,

which drives the total ion flux, by choosing a reduced pulse duration. Boosting the discharge at a specific moment of the discharge, it could favor the preferential ionization of one species over the others. Finally, this will certainly modify the physical and structural properties of the deposited film.

## Acknowledgment

We thank Jordan Champlon, Institute of Technology of Nantes, for his expertise in building the new HiPIMS power supply.

## Conflict of interest

The authors have no conflicts to disclose.

## CRediT (Contribution Roles Taxonomy)

**Joelle Zgheib:** Conceptualization; Data curation; Formal analysis; Investigation; Methodology; Validation; Visualization; Writing - original draft preparation; Writing - review & editing. **Laurent Berthelot:** Methodology. **Julien Tranchant:** Review & editing. **Nicolas Ginot:** Software. **Marie-Paule Besland:** Visualization; Review & editing. **Amael Caillard:** Resources; Review & editing. **Tiberiu Minea:** Resources; Review & editing. **Ahmed Rhallabi:** Funding acquisition; Investigation; Resources; Visualization; Writing – review & editing. **Pierre-Yves Jouan:** Funding acquisition; Investigation; Project administration; Resources; Supervision; Visualization; Writing – review & editing.

## Data Availability

The data supporting this study's findings are available within the article.

## References


[1] M.B. Assouar, O. Elmazria, V. Mortet, P.-Y. Jouan, M.A. Djouadi, and P. Alnot, "Piezoelectric Aluminum Nitride Films Deposited by Triode Sputtering for Surface Acoustic Wave Devices," Ferroelectrics **273**(1), 249–254 (2002).

[2] X.Q. He, G. Brown, K. Demirkan, N. MacKie, V. Lordi, and A. Rockett, "Microstructural and chemical investigation of PVD-CdS/PVD-CuIn1-xGaxSe2 heterojunctions," IEEE J. Photovolt., 1625–1629 (2014).

[3] S. Siegrist, S.-C. Yang, E. Gilshtein, X. Sun, A.N. Tiwari, and F. Fu, "Triple-cation perovskite solar cells fabricated by a hybrid PVD/blade coating process using green solvents," J. Mater. Chem. A **9**(47), 26680–26687 (2021).

[4] R. Bahi, C. Nouveau, N.E. Beliardouh, C.E. Ramoul, S. Meddah, and O. Ghelloudj, "Surface performances of Ti-6Al-4V substrates coated PVD multilayered films in biological environments," Surf. Coat. Technol. **385**, 125412 (2020).

[5] P.E. Hovsepian, A.A. Sugumaran, M. Rainforth, J. Qi, I. Khan, and A.P. Ehiasarian, "Microstructure and load bearing capacity of TiN/NbN superlattice coatings deposited on medical grade CoCrMo alloy by HIPIMS," J. Mech. Behav. Biomed. Mater. **132**, 105267 (2022).

[6] A. Tricoteaux, P.Y. Jouan, J.D. Guerin, J. Martinez, and A. Djouadi, "Fretting wear properties of CrN and Cr2N coatings," Proc. Eight Int. Conf. Plasma Surf. Eng. **174–175**, 440–443 (2003).

[7] J. Keraudy, R.P.B. Viloan, M.A. Raadu, N. Brenning, D. Lundin, and U. Helmersson, "Bipolar HiPIMS for tailoring ion energies in thin film deposition," Surf. Coat. Technol. **359**, 433–437 (2019).

[8] B. Zheng, Z. Wu, B. Wu, Y. Li, and M. Lei, "A global plasma model for reactive deposition of compound films by modulated pulsed power magnetron sputtering discharges," J. Appl. Phys. **121**, 171901 (2017).

[9] M. Čada, Z. Hubička, P. Adámek, J. Klusoň, and L. Jastrabík, "Time-resolved plasma parameters in the HiPIMS discharge with Ti target in Ar/O2 atmosphere," PSE 2010 Spec. Issue **205**, S317–S321 (2011).

[10] E. Wallin, T.I. Selinder, M. Elfwing, and U. Helmersson, "Synthesis of α-Al 2 O 3 thin films using reactive high-power impulse magnetron sputtering," EPL Europhys. Lett. **82**(3), 36002 (2008).

[11] G. Greczynski, and L. Hultman, "Time and energy resolved ion mass spectroscopy studies of the ion flux during high power pulsed magnetron sputtering of Cr in Ar and Ar/N2 atmospheres," Vacuum **84**(9), 1159–1170 (2010).

[12] K. Sarakinos, J. Alami, and S. Konstantinidis, "High power pulsed magnetron sputtering: A review on scientific and engineering state of the art," Surf. Coat. Technol. **204**(11), 1661–1684 (2010).

[13] V. Kouznetsov, K. Macák, J.M. Schneider, U. Helmersson, and I. Petrov, "A novel pulsed magnetron sputter technique utilizing very high target power densities," Surf. Coat. Technol. **122**(2), 290–293 (1999).

[14] K. Macák, V. Kouznetsov, J. Schneider, U. Helmersson, and I. Petrov, "Ionized sputter deposition using an extremely high plasma density pulsed magnetron discharge," J. Vac. Sci. Technol. A **18**(4), 1533–1537 (2000).

[15] U. Helmersson, M. Lattemann, J. Bohlmark, A.P. Ehiasarian, and J.T. Gudmundsson, "Ionized physical vapor deposition (IPVD): A review of technology and applications," Thin Solid Films **513**(1), 1–24 (2006).
[16] P. Raman, J. Weberski, M. Cheng, I. Shchelkanov, and D.N. Ruzic, "A high power impulse magnetron sputtering model to explain high deposition rate magnetic field configurations," J. Appl. Phys. **120**(16), 163301 (2016).
[17] B.C. Zheng, D. Meng, H.L. Che, and M.K. Lei, "On the pressure effect in energetic deposition of Cu thin films by modulated pulsed power magnetron sputtering: A global plasma model and experiments," J. Appl. Phys. **117**(20), 203302 (2015).
[18] J.T. Gudmundsson, J. Alami, and U. Helmersson, "Spatial and temporal behavior of the plasma parameters in a pulsed magnetron discharge," Surf. Coat. Technol. **161**(2), 249–256 (2002).
[19] R. Hippler, M. Cada, and Z. Hubicka, "Time-resolved Langmuir probe diagnostics of a bipolar high power impulse magnetron sputtering discharge," Appl. Phys. Lett. **116**(6), 064101 (2020).
[20] R. Hippler, M. Cada, V. Stranak, and Z. Hubicka, "Time-resolved optical emission spectroscopy of a unipolar and a bipolar pulsed magnetron sputtering discharge in an argon/oxygen gas mixture with a cobalt target," Plasma Sources Sci. Technol. **28**(11), 115020 (2019).
[21] A. Ferrec, J. Kéraudy, and P.-Y. Jouan, "Mass spectrometry analyzes to highlight differences between short and long HiPIMS discharges," Appl. Surf. Sci. **390**, 497–505 (2016).
[22] D. Lundin, T. Minea, and J.T. Gudmundsson, *High Power Impulse Magnetron Sputtering: Fundamentals, Technologies, Challenges and Applications*, Elsevier (2020).
[23] T. Kubart, M. Čada, D. Lundin, and Z. Hubička, "Investigation of ionized metal flux fraction in HiPIMS discharges with Ti and Ni targets," Surf. Coat. Technol. **238**, 152–157 (2014).
[24] K. Bobzin, N. Bagcivan, P. Immich, S. Bolz, J. Alami, and R. Cremer, "High Power Impulse Magnetron Sputtering – HIPIMS," J Mater Process Technol, 165 (2008).
[25] O. Antonin, V. Tiron, C. Costin, G. Popa, and T.M. Minea, "On the HiPIMS benefits of multi-pulse operating mode," J. Phys. Appl. Phys. **48**(1), 015202 (2014).
[26] M. Fekete, J. Hnilica, C. Vitelaru, T. Minea, and P. Vašina, "Ti atom and Ti ion number density evolution in standard and multi-pulse HiPIMS," J. Phys. Appl. Phys. **50**(36), 365202 (2017).
[27] P. Souček, J. Hnilica, P. Klein, M. Fekete, and P. Vašina, "Microstructure of titanium coatings controlled by pulse sequence in multipulse HiPIMS," Surf. Coat. Technol. **423**, 127624 (2021).
[28] N. Britun, M. Michiels, T. Godfroid, and R. Snyders, "Ion density evolution in a high-power sputtering discharge with bipolar pulsing," Appl. Phys. Lett. **112**(23), 234103 (2018).
[29] I.-L. Velicu, G.-T. Ianoş, C. Porosnicu, I. Mihăilă, I. Burducea, A. Velea, D. Cristea, D. Munteanu, and V. Tiron, "Energy-enhanced deposition of copper thin films by bipolar high power impulse magnetron sputtering," Surf. Coat. Technol. **359**, 97–107 (2019).
[30] G. Y. Yushkov and A. Anders, "Origin of the Delayed Current Onset in High-Power Impulse Magnetron Sputtering," IEEE Trans. Plasma Sci. **38**(11), 3028–3034 (2010).
[31] H. Ji, G.S. Was, J.W. Jones, and N.R. Moody, "Effect of ion bombardment on in-plane texture, surface morphology, and microstructure of vapor deposited Nb thin films," J. Appl. Phys. **81**(10), 6754–6761 (1997).
[32] D.M. Mattox, "Particle bombardment effects on thin- film deposition: A review," J. Vac. Sci. Technol. A **7**(3), 1105–1114 (1989).

[33] F. Cemin, M. Tsukamoto, J. Keraudy, V.G. Antunes, U. Helmersson, F. Alvarez, T. Minea, and D. Lundin, "Low-energy ion irradiation in HiPIMS to enable anatase TiO2 selective growth," J. Phys. Appl. Phys. **51**(23), 235301 (2018).
[34] F. Cemin, G. Abadias, T. Minea, and D. Lundin, "Tuning high power impulse magnetron sputtering discharge and substrate bias conditions to reduce the intrinsic stress of TiN thin films," Spec. Issue "Thin Film Adv. Dedic. 75th Birthd. Profr. Joe Greene **688**, 137335 (2019).
[35]"Impedans," (n.d.).
[36] A. Rousseau, E. Teboul, and S. Béchu, "Comparison between Langmuir probe and microwave autointerferometry measurements at intermediate pressure in an argon surface wave discharge," J. Appl. Phys. **98**(8), 083306 (2005).
[37] J.T. Gudmundsson, D. Lundin, N. Brenning, M.A. Raadu, C. Huo, and T.M. Minea, "An ionization region model of the reactive Ar/O2high power impulse magnetron sputtering discharge," Plasma Sources Sci. Technol. **25**(6), 065004 (2016).
[38] J. Zgheib, P.Y. Jouan, and A. Rhallabi, "A high-power impulse magnetron sputtering global model for argon plasma–chromium target interactions," J. Vac. Sci. Technol. A **39**(4), 043004 (2021).
[39] P. Poolcharuansin, and J.W. Bradley, "Short- and long-term plasma phenomena in a HiPIMS discharge," Plasma Sources Sci. Technol. **19**(2), 025010 (2010).
[40] A. Vetushka, and A.P. Ehiasarian, "Plasma dynamic in chromium and titanium HIPIMS discharges," J. Phys. Appl. Phys. **41**(1), 015204 (2007).
[41] J.T. Gudmundsson, P. Sigurjonsson, P. Larsson, D. Lundin, and U. Helmersson, "On the electron energy in the high power impulse magnetron sputtering discharge," J. Appl. Phys. **105**(12), 123302 (2009).
[42] J.T. Gudmundsson, D. Lundin, G.D. Stancu, N. Brenning, and T.M. Minea, "Are the argon metastables important in high power impulse magnetron sputtering discharges?," Phys. Plasmas **22**(11), 113508 (2015).
[40] A. Revel, T. Minea, and S. Tsikata "Pseudo-3D PIC modeling of drift-induced spatial inhomogeneities in planar magnetron plasmas" Phys. Plasmas 23, 100701 (2016).